The Purple Mixed-Valence Cu_A Center in Nitrous-oxide Reductase: EPR of the Copper-63-, Copper-65-, and Both Copper-65- and [^{15}N]Histidine-Enriched Enzyme and a Molecular Orbital Interpretation

Frank Neese,[†] Walter G. Zumft,[‡] William E. Antholine,[§] and Peter M. H. Kroneck*,[†]

Contribution from the Fakultät für Biologie, Universität Konstanz, D-78434 Konstanz, Germany, Lehrstuhl für Mikrobiologie, Universität Fridericiana, D-76128 Karlsruhe, Germany, and Biophysics Research Institute, Medical College of Wisconsin, 8701 Watertown Plank Road, Milwaukee, Wisconsin 53226

Received January 16, 1996[⊗]

Abstract: EPR spectra for the purple mixed-valence [$Cu^{1.5+}$...$Cu^{1.5+}$], $S = {}^1/_2$, site (Cu_A) in nitrous-oxide reductase (N_2OR) were obtained after insertion of either ^{63}Cu or ^{65}Cu or both ^{65}Cu and [^{15}N]histidine. The spectrum of ^{65}Cu- and [^{15}N]histidine-enriched N_2OR improved the resolution of the Cu hyperfine lines, but no lines from nitrogen and proton couplings were resolved. The Cu hyperfine parameters obtained by a theory analogous to that of Maki and McGarvey were indicative of a highly covalent Cu site. The total Cu character ($Cu_{A1} + Cu_{A2}$) in the ground state wave function required to describe the spin density distribution was 31−37% compared to 41% for type-1 Cu in plastocyanin. This value does not completely account for the reduction of g_{max} from 2.23 of type-1 Cu in plastocyanin to 2.18 of Cu_A. Remaining discrepancies were discussed in terms of different alignments of the principal axes for the hypothetical monomeric Cu_{A1} and Cu_{A2} in [$Cu^{1.5+}$...$Cu^{1.5+}$]. This effect appeared in the simulations of the EPR spectra as a noncoincidence between the Cu hyperfine and *g* principal axis systems. The *g*-value analysis of Cu_A predicts an electric dipole forbidden absorption band in the near-infrared region. Based on X-ray structural data of Cu_A in cytochrome *c* oxidase, iterative extended Hückel and UHF-INDO/S calculations on a sulfur-bridged $[(NH_3)Cu^{1.5+}(SCH_3)_2Cu^{1.5+}(NH_3)]^+$ core were used to interpret the EPR results. The ground state was selected as $^2B_{3u}$ and not $^2B_{2u}$, because $^2B_{2u}$ has very little spin density (<0.5%) on the coordinated nitrogen atoms, which contradicts the experimental value of 3−5% spin density found on N_{His}.

Introduction

Nitrous-oxide reductase (N_2OR; EC 1.7.99.6) is the terminal oxidoreductase in a respiratory chain converting N_2O to N_2 in denitrifying bacteria,[1] eq 1. As isolated, N_2OR from *Pseudomonas stutzeri* is a purple enzyme with an intense absorption maximum at 540 nm (ϵ = 14−18 mM^{-1} cm^{-1}) and a characteristic continuous wave electron paramagnetic resonance (CW EPR) spectrum (X-band) with an unusual seven-line hyperfine pattern in the g_{II} region. The protein consists of two identical subunits with 4 Cu/M_r 65.800. A catalytically inactive protein was isolated from the mutant MK402 which contained up to 4 Cu/dimeric protein.[2,3] Interest in N_2OR is directly related to its unique spectral properties and to its similarity to the Cu_A center of cytochrome *c* oxidase (COX; EC 1.9.3.1). It had been stated that the Cu_A site is different from any other,[4] and a mononuclear $Cu^{II}2S_{Cys,}2N_{His}$ site was proposed to explain the unusual properties of this site.[5,6] The suggestion of a dinuclear mixed-valent nature for Cu_A in COX based on the EPR spectroscopic properties of N_2OR had generated some controversy[7−11] but became finally settled with the crystallographic structure of COX from *Paracoccus denitrificans* and from bovine heart.[12,13]

$$N_2O + 2H^+ + 2e^- \rightarrow N_2 + H_2O \qquad E_0'(N_2O/N_2) = 1.35\ V \quad (1)$$

The Cu(II) centers in proteins have been classified into three types based on their optical and EPR properties.[14] These are the "blue" (type-1), "nonblue" (type-2), and "dinuclear" (type-3) Cu centers. Crystal structures at high resolution are available

* To whom correspondence should be addressed: Fakultät für Biologie, Universität Konstanz, Postfach 5560 M665, D-78434 Konstanz, Germany. Phone: (49)7531-882103. Fax: (49)7531-882966. E-mail: Peter.Kroneck@uni-konstanz.de.

[†] Universität Konstanz.

[‡] Universität Fridericiana.

[§] Medical College of Wisconsin.

[⊗] Abstract published in *Advance ACS Abstracts,* August 15, 1996.

(1) (a) Zumft, W. G.; Kroneck, P. H. H. *Denitrification in soil and sediment*; Revsbech, N. P., Sörensen, J., Eds.; Plenum Press: New York, 1990; pp 37−55. (b) Zumft, W. G.; Kroneck, P. M. H. *Adv. Inorg. Biochem.* **1996**, *11*, 1993.

(2) Coyle, C. L.; Zumft, W. G.; Kroneck, P. M. H.; Körner, H.; Jakob, W. *Eur. J. Biochem.* **1985**, *153*, 459.

(3) Riester, J.; Zumft, W. G.; Kroneck, P. M. H. *Eur. J. Biochem.* **1989**, *178*, 751.

(4) Mims, W. B.; Peisach, J.; Shaw, R. W.; Beinert, H. *J. Biol. Chem.* **1980**, *255*, 6843.

(5) Chan, S. I.; Li, P. M. *Biochemistry* **1990**, *29*, 1.

(6) George, G. N.; Cramer, S. P.; Frey, T. G.; Prince, R. C. *Biochem. Biophys. Acta* **1993**, *1142*, 240.

(7) Li, P. M.; Malmström, B. G.; Chan, S. I. *FEBS Lett.* **1989**, *248*, 210.

(8) Kroneck, P. M. H.; Antholine, W. E.; Riester, J.; Zumft, W. G. *FEBS Lett.* **1989**, *248*, 212.

(9) Malmström, B. G. *Arch. Biochem. Biophys.* **1990**, *280*, 233.

(10) Palmer, G. *J. Bioenerg. Biomembr.* **1993**, *25*, 145.

(11) Malmström, B. G.; Aasa, R. *FEBS Lett.* **1993**, *325*, 49.

(12) (a) Iwata, S.; Ostermeier, C.; Ludwig, B.; Michel, H. *Nature* **1995**, *376*, 660. (b) Wilmanns, M.; Lappalainen, P.; Kelly, M.; Sauer-Eriksson, E.; Saraste, M. *Proc. Natl. Acad. Sci. U.S.A. 92*, 11955.

(13) Tsukihara, T.; Aoyama, H.; Yamashita, E.; Tomizaki, T.; Yamaguchi, H.; Shinzawa-Itoh, K.; Nakashima, R.; Yaono, R.; Yoshikawa, S. *Science* **1995**, *269*, 1069.

(14) Malkin, R.; Malmström, B. G. *Adv. Enzymol.* **1970**, *33*, 177.

S0002-7863(96)00125-4 CCC: $12.00

for the three types, and most Cu sites in proteins can be described within this scheme. Clearly, two exceptions from this picture exist, and these are the EPR-detectable Cu centers of COX and N_2OR with unusually low *g*-values at 2.18, 2.02, and 2.00 and small Cu hyperfine couplings.[15] This fact becomes evident by plotting the EPR parameters g_{II} vs A_{II} of the various Cu proteins.[3,11,16,17]

If one assumes two identical subunits for N_2OR from *P. stutzeri*, each carrying four Cu atoms, then the metals can be arranged in two dinuclear centers: (i) the EPR-detectable, mixed-valence $[Cu^{1.5+}...Cu^{1.5+}]$, $S = {}^1/_2$, Cu_A site, and (ii) the EPR-silent, antiferromagnetically coupled $[Cu^{2+}...Cu^{2+}]$, Cu_z site. This model is mainly based on the molecular properties of the enzyme as isolated and the properties of the mutant MK402 protein from *P. stutzeri* including (i) the relative molecular mass, the number of subunits, and the primary structure of N_2OR; (ii) the total Cu content and the concentration of EPR-detectable Cu in native, semireduced, and fully reduced N_2OR; (iii) the parameters obtained from multifrequency CW EPR, electron spin echo envelope modulation (ESEEM), UV−vis, circular dichroism (CD), magnetic circular dichroism (MCD), extended X-ray absorption fine structure (EXAFS), and resonance Raman spectroscopy; and (iv) the magnetic properties as determined by SQUID susceptometry.[2,3,15,18−25] Multifrequency EPR spectroscopy, *g*-factor analysis, and computer simulation of the EPR spectra were used to propose a dinuclear mixed-valence $S = {}^1/_2$ site with a core $2Cu^{1.5+}2S_{Cys},2N_{His}$ as opposed to the "classical" mononuclear site found in type-1 Cu proteins, i.e., a $Cu^{II}SCys,2N_{His},S_{Met}$ center, or the "Chan" model $Cu^{II}2S_{Cys},2N_{His}$.[5,15,19,26]

A homologous domain, extending over at least 50 amino acid residues, is shared among the N_2OR from *P. stutzeri*, *P. aeruginosa*, and *Alcaligenes eutrophus*, and a Cu_A-binding region of the COX subunit II.[25,27−29] Two conserved cysteines, two histidines, one methionine, one aspartate, one valine, and two aromatic residues are part of the Cu_A consensus sequence.

An artificial Cu_A site was engineered into the C-terminal fragment of the membrane-bound CyoA subunit of the *Escherichia coli* cytochrome *o* quinol oxidase.[27] In a similar approach, the Cu_A domains of *P. denitrificans* COX and of the *caa3*-type oxidase from *Bacillus subtilis* were expressed in a water-soluble form.[30,31] Site-directed mutagenesis of the engineered CyoA fragment from *E. coli* indicated that two cysteines (Cys 207 and Cys 211), two histidines (His 172 and His 215), and one methionine (Met 218) are the major Cu ligands of a purple dinuclear Cu_A center,[29,32] as proposed in the earlier model for the Cu_A center of bacterial N_2OR[15,25] and of mammalian COX.[28] Note that the CW X-band EPR spectra of bacterial and mammalian COX, as well as of the engineered soluble Cu_A fragments, do not show the well-resolved seven-line pattern in the g_{II} region around $g = 2.18$ as described for purple N_2OR.[2,3,15,27,30−33] Some resolution enhancement was achieved by using the second-harmonic display, or pseudomodulation treatment of the EPR spectra of COX.[15,34] Possibly, the g_{II} region for COX is not resolved because (i) the g_{mid} component of the heme *a* is superimposed onto the lines at g_{II} and (ii) the interaction of Fe(III) sites in COX but not in N_2OR affects the resolution of the lines. In the case of the Cu_A fragments which had been expressed in *E. coli* and reconstituted with $Cu^{II}Cl_2$,[27,30,31] EPR signals from adventitious Cu were superimposed on the spectrum of the mixed-valence Cu_A center. Even at S-band (3.959 GHz), the resolution was poor compared to that of the EPR spectra (frequency range 2.7−9.50 GHz) reported for purple N_2OR and the MK402 mutant protein from *P. stutzeri*.[15,31]

Here we present an EPR analysis of the Cu_A site in N_2OR which has been labeled by insertion of either ^{63}Cu or ^{65}Cu isotopes or both ^{65}Cu and [^{15}N]histidine to confirm the mixed-valence character, $[Cu^{1.5+}...Cu^{1.5+}]$, $S = {}^1/_2$, of the Cu_A site in N_2OR. Compared to earlier attempts,[15] the interpretation and simulation of the EPR spectra were significantly improved by applying mixed-valence theory. Based on the crystallographic analysis of the Cu_A center in COX,[12,13] iterative extended Hückel (IEHT) and unrestricted Hartree−Fock intermediate neglect of differential overlap/spectroscopic parametrization (UHF-INDO/S) calculations on a planar $[(NH_3)Cu^{1.5+}(SCH_3)_2Cu^{1.5+}(NH_3)]^+$ core were used to interpret the EPR spectroscopic results, including the unusually low *g*-values of Cu_A, and to understand the highly delocalized character of the mixed-valence center.

Experimental Section

Chemicals. Racemic D,L-[1,3-$^{15}N_2$]histidine was obtained from the NIH National Stable Isotope Resource, Los Alamos, NM. Metallic ^{63}Cu and ^{65}Cu were purchased from Cambridge Isotope Laboratories, Woburn, MA.

Preparation of Isotope-Enriched Nitrous-oxide Reductase. Cu labeling was done by in vivo incorporation of the desired isotope into a growing culture of *P. stutzeri* ZoBell (ATCC 14405). The synthetic asparagine−citrate medium was prepared with deionized water and contained the previously specified ingredients, except for $CuSO_4$.[2] The pH of the medium was initially adjusted to 6.8 and kept during growth at an upper limit of 7.2 with 1 M HCl. Cu was added as the ^{63}Cu or ^{65}Cu isotope to give a final concentration of 10 μM (10-fold excess over the standard growth concentration). Metallic Cu (approximately

(15) Antholine, W. E.; Kastrau, D. H. W.; Steffens, G. C. M.; Zumft, W. G.; Kroneck, P. M. H. *Eur. J. Biochem.* **1992**, *209*, 875.
(16) Vänngård, T. *Biological applications of electron spin resonance*; Swartz, H. M., Bolton, J. R., Borg, D. C., Eds.; Wiley-Interscience: New York, London, Sidney, Toronto, 1972; pp 411−447.
(17) Peisach, J.; Blumberg, W. E. *Arch. Biochem. Biophys.* **1974**, *165*, 691.
(18) Dooley, D. A.; Moog, R. S.; Zumft, W. G. *J. Am. Chem. Soc.* **1987**, *109*, 6730.
(19) (a) Kroneck, P. M. H.; Antholine, W. E.; Riester, J.; Zumft, W. G. *FEBS Lett.* **1988**, *242*, 70. (b) Kroneck, P. M. H.; Antholine, W. E.; Kastrau, D. H. W.; Buse, G.; Steffens, G. C. M.; Zumft, W. G. *FEBS Lett.* **1990**, *268*, 274.
(20) Jin, H.; Thomann, H.; Coyle, C. L.; Zumft, W. G. *J. Am. Chem. Soc.* **1989**, *111*, 4262.
(21) Scott, R. A.; Zumft, W. G.; Coyle, C. L.; Dooley, D. M. *Proc. Natl. Acad. Sci. U.S.A.* **1989**, *86*, 4082.
(22) Farrar, J. A.; Thomson, A. J.; Cheesman, M. R.; Dooley, D. M.; Zumft, W. G. *FEBS Lett.* **1991**, *294*, 11.
(23) Dooley, D. M.; McGuirl, M. A.; Rosenzweig, A. C.; Landin, J. A.; Scott, R. A.; Zumft, W. G.; Devlin, F.; Stephens, P. J. *Inorg. Chem.* **1991**, *30*, 3006.
(24) Dooley, D. M.; Landin, A. C.; Rosenzweig, A. C.; Zumft, W. G.; Day, E. P. *J. Am. Chem. Soc.* **1991**, *113*, 8978.
(25) Zumft, W. G.; Dreusch, A.; Löchelt, S.; Cuypers, H.; Friedrich, B.; Schneider, B. *Eur. J. Biochem.* **1992**, *208*, 31.
(26) Kroneck, P. M. H.; Riester, J.; Zumft, W. G.; Antholine, W. E. *Biol. Met.* **1990**, *3*, 103.
(27) Van der Oost, J.; Lappalainen, P.; Musachio, A.; Warne, A.; Lemieux, L.; Rumbley, J.; Gennis, R. B.; Aasa, R.; Pascher, T.; Malmström, B. G.; Saraste, M. *EMBO J.* **1992**, *11*, 3209.
(28) Steffens, G. C. M.; Soulimane, T.; Wolf, G.; Buse, G. *Eur. J. Biochem.* **1993**, *213*, 1149.
(29) Kelly, M.; Lappalainen, P.; Talbo, G.; Haltia, T.; Van der Oost, J.; Saraste, M. *J. Biol. Chem.* **1993**, *268*, 16781.
(30) Lappalainen, P.; Aasa, R.; Malmström, B. G.; Saraste, M. *J. Biol. Chem.* **1993**, *268*, 26416.
(31) Von Wachenfeldt, C.; de Vries, S.; van der Oost, J. *FEBS Lett.* **1994**, *340*, 109.
(32) Farrar, J. A.; Lappalainen, P.; Zumft, W. G.; Saraste, M.; Thomson, A. J. *Eur. J. Biochem.* **1995**, *232*, 294.
(33) Beinert, H.; Griffith, D. E.; Wharton, D. C.; Sands, R. H. *J. Biol. Chem.* **1962**, *237*, 2337.
(34) Kroneck, P. M. H.; Antholine, W. E.; Koteich, H.; Kastrau, D. H. W.; Neese, F.; Zumft, W. G. *Bioinorganic Chemistry of Copper*; Karlin, K. D., Tyeklár, Z., Eds.; Chapman & Hall: New York, 1993; pp 419−426.

100 mg, purity 99.7%) was dissolved in concentrated HCl, containing a few drops of concentrated HNO_3, and was made up to 100 mL with quartz-distilled water.[35] Cells were grown in batch culture which, starting from 1 L, was scaled up two times by a factor of 10. The two initial stages were grown O_2-limited. In the last stage N_2OR was induced by nitrate which was grown for 24 h as an anaerobic fed-batch system with ca. 300 g of $NaNO_3$. Cells were harvested in a continuous-flow centrifuge, washed once in cold 50 mM Tris/HCl, pH 7.5, 50 mM $MgCl_2$, and used immediately for enzyme preparation.

To label N_2OR with [^{15}N]histidine an auxotrophic mutant was generated by random transposon Tn5 mutagenesis.[36] Kanamycin-resistant strains were screened for histidine auxotrophy by replica platting. The His$^-$ strain MK608 was used for labeling N_2OR with [^{15}N]histidine and for double labeling with ^{65}Cu and [^{15}N]histidine. The minimum amount of D,L-histidine for obtaining sufficient biomass for enzyme preparation from the culture medium was 40 mg L^{-1}. N_2OR was prepared as detailed previously under anaerobic conditions except for isoelectric focusing.[2]

CW EPR. EPR spectra at X- (9.3 GHz), S- (2.4−3.7 GHz), and C-bands (4.6 GHz) were recorded as described earlier.[15] The instrumentation included a gaussmeter for magnetic field calibration and a frequency counter. Loop-gap resonators and low-frequency microwave bridges designed and built at the National Biomedical ESR Center (Medical College of Wisconsin, Milwaukee, WI) were used. Temperatures of 5−50 K were maintained with a helium-flow system (Air Products, Allentown, PA). EPR spectra were recorded at 100 KHz modulation, the amplitude was 2−5 G, and the power was less than the power to saturate. Experimental data were processed with the Bruker software or the program SUMSPEC.[37] The amount of EPR-detectable Cu was determined according to Vänngård.[16] Protein samples were transferred to standard EPR quartz tubes (outer diameter 4.0 mm for 2.4−9.3 GHz) and frozen in liquid nitrogen.

Computer Simulation of EPR Spectra. EPR spectra were simulated with the program EPR.[38] The program solves the spin Hamiltonian eigenvalue problem to first order in perturbation theory (eq 2). The program allows for extensive least squares minimization

$$\hat{H}_{\mathrm{Sp}} = \beta \vec{H}\mathbf{g}\hat{S} + \hat{S}\mathbf{D}\hat{S} + \sum_i \hat{S}\mathbf{A}^{(i)}\hat{I}_i \qquad (2)$$

and simulations in field and g space.[39] In eq 2 nuclear Zeeman and quadrupole effects are neglected; all other symbols have the usual meaning. Unless stated otherwise, the EPR spectra of the ^{65}Cu-enriched N_2OR were used for reference in the simulations. Preliminary simulations showed no particular advantage of g space over field space calculations; thus all simulations were performed on a linear magnetic field scale assuming a Gaussian line shape as results from unresolved hyperfine splittings. The program incorporates an empirical expression for the spectral line width (eqs 3a,b). W is the residual line width in

$$W(m_I^{(1)}...m_I^{(n)}) = \frac{1}{g^2}\sqrt{l_x^2 g_x^4 \Omega_x^2 + l_y^2 g_y^4 \Omega_y^2 + l_z^2 g_z^4 \Omega_z^2} \qquad (3a)$$

$$\Omega_i = W_i + c_1 \nu + \sum_i \epsilon_i m_{I,i} + c_2 m_{I,i}^2 \qquad (3b)$$

gauss, l_i's are the direction cosines, $m_{I,i}$ is the nuclear quantum number for the ith nucleus, c_1 describes the dependence of the line width on the spectrometer frequency ν, and c_2 and ϵ describe the line width terms which are quadratic and linear in the nuclear spin quantum numbers. Similar equations are used by many investigators (ref 40 is recommended for review).

MO Calculations. MO calculations at the extended Hückel and iterative extended Hückel level[41] were carried out using parameters from Keijzers and DeBoer.[42] Furthermore, UHF-INDO/S[43] calculations using a locally developed program[44] were employed. A value of 20 eV was assumed for β_d^0(Cu) instead of the 51 eV value used in the original parametrization.[43c] This reduction was strongly suggested from calculations on the optical and magnetic properties of small Cu(II) complexes including $[CuCl_4]^{2-}$ (F. Neese, P. M. H. Kroneck, to be published). The diagonal elements for a given atom in the iterative extended Hückel method depend on its Mulliken charge Q_A (eq 4). α,

$$H_{ii}^{AA} = \alpha_i + \beta_i k Q_A + \gamma_i k^2 Q_A^2 \qquad (4)$$

β, and γ depend on the atom and the orbital angular momentum quantum number. The parameter k[42] is introduced to damp the charge dependence of the diagonal elements to avoid too much charge equilibration in the iteration process. The off-diagonal elements were calculated by the Wolfsberg−Helmholtz relation.[45] Usually, the Hückel parameter K takes a value of 1.75.[41] However, Keijzers and DeBoer found in their study of Cu(II) dithiocarbamate complexes that $K = 2.5$ would give the best fit of the EPR results, which was also found by us. Note that this choice is required to obtain the correct SOMO orbital for the nearly orbitally degenerate type-1 Cu model. For an estimate of the atomic spin density we treated our MOs as if they would have been obtained from a spin-restricted open-shell Longuett−Higgins−Pople (LHP) wave function,[46] and the resultant spin density matrix was used in a Mulliken type analysis.[47] Coordinated amino acid residues were mimicked as follows: thiolate sulfur (cysteine) by $-SCH_3$, imidazole nitrogen (histidine) by NH_3, thioether sulfur (methionine) by $-S(CH_3)_2$, and carboxylate oxygen (aspartate, glutamate) by $HCOO^-$. The geometry for the type-1 copper in plastocyanin was taken from Lowery and Solomon,[48] and the structural data for the mixed-valence dicopper(I,II) complex $[Cu_2L]^{3+}$ {L = $N[CH_2CH_2N(H)CH_2CH_2N(H)CH_2CH_2]_3N$} from Barr et al.,[49] in this case, the coordinated nitrogen atoms were mimicked by NH_3.

Results

Electron Paramagnetic Resonance. The pattern that identifies the EPR-detectable site in native nitrous-oxide reductase is the seven lines in the g_{II} region of the spectrum at X-band (Figure 1). The apparent hyperfine coupling A_{II} (38 G) is unusually small, with approximately 60% of the value expected for the type-1 Cu.[14] The spectra of N_2OR with a single isotope of either ^{63}Cu or ^{65}Cu rule out the possibility that the lines of the protein with naturally abundant Cu arise from a ^{63}Cu monomer (69% natural abundance) and a ^{65}Cu monomer (31% natural abundance) instead of the superimposition of the Cu pairs [$^{63}Cu^{1.5+}$...$^{63}Cu^{1.5+}$] (47%), [$^{63}Cu^{1.5+}$...$^{65}Cu^{1.5+}$] (42.6%), and [$^{65}Cu^{1.5+}$...$^{65}Cu^{1.5+}$] (9.5%).[50] A significant reduction in line width in the ^{65}Cu and [^{15}N]histidine double-labeled N_2OR, compared to the spectrum of the ^{65}Cu-enriched enzyme, was

(35) Van de Bogart, M.; Beinert, H. *Anal. Biochem.* **1967**, *20*, 325.
(36) Zumft, W. G.; Döhler, K.; Körner, H. *J. Bacteriol.* **1985**, *163*, 918.
(37) Hyde, J. S.; Pasenkiewicz-Gierula, M.; Jesmanowicz, A.; Antholine, W. E. *Appl. Magn. Reson.* **1990**, *1*, 483.
(38) Neese, F. QCPE program no. QCMP 136.
(39) Hagen, W. R. *Advanced EPR—applications in biology and biochemistry*; Hoff, A. J., Ed.; Elsevier: Amsterdam, Oxford, New York, Tokyo, 1989; pp 785−811.
(40) Pilbrow, J. R. *Transition ion electron paramagnetic resonance*; Oxford Science Publications: Oxford, 1990.
(41) (a) Hoffmann, R. *J. Chem. Phys.* **1963**, *39*, 1397. (b) Zerner, M. C.; Gouterman, M. *Theor. Chim. Acta* **1966**, *4*, 44. (c) Duke, B. J. *Theor. Chim. Acta* **1968**, *9*, 260.
(42) Keijzers, C. P.; DeBoer, E. *Mol. Phys.* **1974**, *29*, 1007.
(43) (a) Bacon, A. D.; Zerner, M. C. *Theor. Chim. Acta* **1979**, *53*, 21. (b) Zerner, M. C.; Loew, G. H.; Kirchner, R. F.; Mueller-Westerhoff, U. T. *J. Am. Chem. Soc.* **1980**, *102*, 589. (c) Anderson, W. P.; Edwards, W. D.; Zerner, M. C. *Inorg. Chem.* **1986**, *25*, 2728−2732.
(44) Neese, F. Manuscript in preparation.
(45) Wolfsberg, M.; Helmholtz, L. *J. Chem. Phys.* **1952**, *20*, 837.
(46) (a) Longuett-Higgins, H. C.; Pople, J. A. *Proc. Phys. Soc.* **1955**, *86A*, 591 (b) Dewar, M. J.; Hashmall, J. A.; Venier, C. G. *J. Am. Chem. Soc.* **1968**, *90*, 1953.
(47) (a) Mulliken, R. S. *J. Chem. Phys.* **1955**, *23*, 1833, (b) 1841, (c) 2338, (d) 2343.
(48) Lowery, M. D.; Solomon, E. I. *Inorg. Chim. Acta* **1992**, *198−200*, 233.
(49) Barr, M. E.; Smith, P. H.; Antholine, W. E.; Spencer, B. *J. Chem. Soc., Chem. Commun.* **1993**, 1649.
(50) Kaim, W.; Moscherosch, M. *J.* Chem. *Soc., Faraday Trans.* **1991**, *87*, 3185.

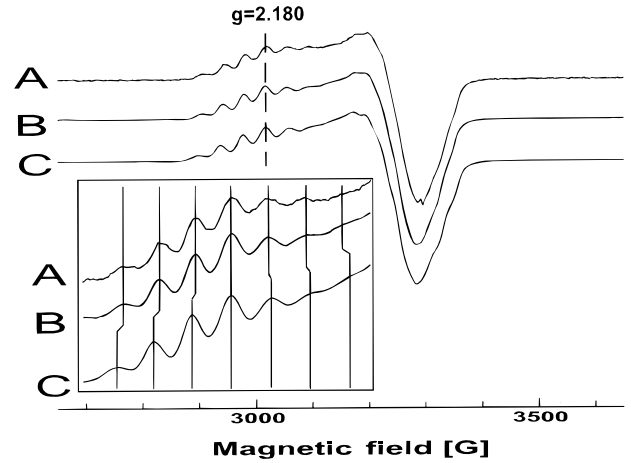

Figure 1. X-band CW EPR spectra of (A) $^{63/65}$Cu natural abundance and (B) ^{63}Cu- and (C) ^{65}Cu-enriched N_2OR from *P. stutzeri*: temperature, 10 K; power, 200 μW; microwave frequency, 9.241 28 GHz; modulation amplitude, 4 G. The inset shows an expansion of the g_{II} region with line shifts due to Cu isotope substitution.

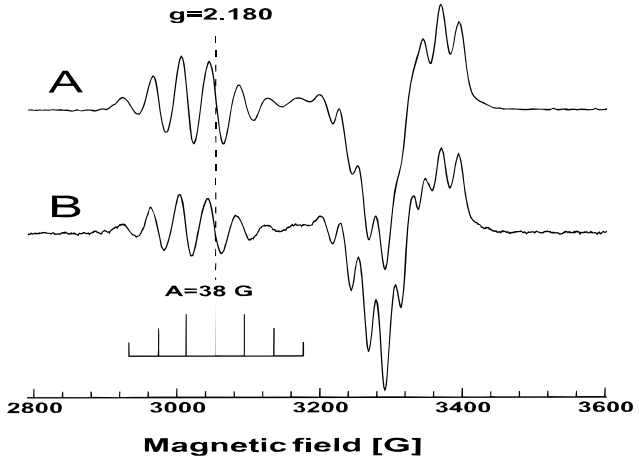

Figure 2. X-band CW EPR spectra (second-harmonic display) of (A) ^{65}Cu-enriched and (B) ^{65}Cu- and [^{15}N]histidine-enriched N_2OR from *P. stutzeri*. Experimental conditions as in Figure 1.

detected in both the g_{II} and g_I regions (Figure 2). This narrowing of the line width suggests the presence of unresolved hyperfine lines from N_{His} coordinated to the Cu_A site, as previously reported for Cu_A in COX.[51,52] A significant improvement in resolution of the EPR spectra at lower frequencies, i.e., 2.4−3.7 GHz (S-band) or 4.6 GHz (C-band), was not obtained.

Simulation of EPR Spectra. The strategy to simulate the EPR spectra of N_2OR followed first the "traditional" approach, where the spectrum was fitted to the spin Hamiltonian[15] (eq 2, $S = {}^1/_2$ system, two Cu nuclei with $I = {}^3/_2$). The fits were improved by the application of mixed-valence theory[53] to EPR spectroscopy as derived in the supporting information.

A. Fitting of the EPR Spectra to the Spin Hamiltonian. An iterative strategy for the simulation of the multifrequency EPR spectra of N_2OR was adopted. Starting from a restricted set of assumptions (axial EPR spectra; *vide infra*), these were

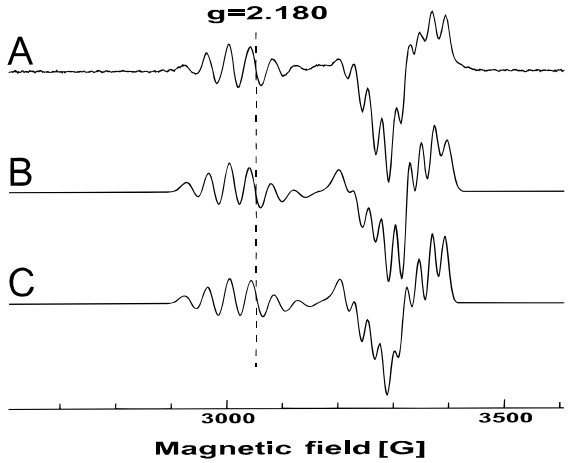

Figure 3. Experimental (A) and simulated X-band CW EPR spectra of ^{65}Cu- and [^{15}N]histidine-enriched N_2OR from *P. stutzeri*. (B) Simulation with noncollinear g and A axes, and Cu hyperfine tensors tilted by the Euler angles $(1/2)\bar{\beta} = \pm 17°$ respectively; parameters in Table 2. (C) Simulation with collinear g and A axes; parameters in Table 1.

Table 1. Best Fit Parameters for the Simulation of the X-Band EPR Spectrum of ^{65}Cu- and [^{15}N]Histidine-Enriched N_2OR from *P. stutzeri*[a]

	g	$\mathbf{A}^{CuA1}$ (MHz)	$\mathbf{A}^{CuA2}$ (MHz)	W (G)	c_2 (G/MHz)	ϵ (G^2/MHz)
g_{min}	2.007	59	68	13.5	0.2	0.0030
g_{mid}	2.024	60	68	12.5	0.3	−0.0011
g_{max}	2.180	117	123	13.5	7.8	−0.0085

[a] Collinear **g** and **A** tensors were used.

released one at a time. The effect was judged from the root mean square deviation between the simulated and the experimental spectrum. The first simulations employed purely axial EPR spectra ($g_{min} = g_{mid} = g_I$; $\mathbf{A}^{CuA1} = \mathbf{A}^{CuA2}$; $\Delta\mathbf{A} = \mathbf{A}^{CuA1} - \mathbf{A}^{CuA2}$; $A^{Cu}_{min} = A^{Cu}_{mid} = A_I$; $A^{Cu}_{max} = A_{II}$) with starting parameters taken from the experimental spectra ($g_{II} = 2.180$, $g_I = 2.010$, $A_{II} = 120$ MHz, $A_I = 75$ MHz). These restrictions did not result in satisfactory fits at all frequencies, especially at high magnetic field in the $g_\perp$ region (Figure 3). The X-band spectrum of the ^{65}Cu- and [^{15}N]histidine-enriched enzyme showed the highest resolution in this region (Figure 2). To reproduce these spectral features in the simulation it was necessary to allow for $g_{min} \neq g_{mid}$, $\mathbf{A}^{CuA1} \neq \mathbf{A}^{CuA2}$, and $A_{min} \neq A_{mid}$. A least squares fit starting from different initial values always converged to a set of values of $A_{min} = 63.5$ MHz, $A_{mid} = 64$ MHz, and $\Delta A_{min} = 9$ MHz, $\Delta A_{mid} = 4$ MHz. This set of data gave a satisfactory fit with regard to the line positions at X-, C-, and S-bands, but the intensities were not met for each individual line. Thus, the minimum requirements for a satisfactory fit were rhombic **g** and **A** tensors with slightly different hyperfine tensors for the two Cu centers. Further progress was achieved by variation of the line width with the nuclear hyperfine quantum numbers m_{I1} and m_{I2}. The variation of the line width within the seven-line pattern could be satisfactorily accounted for by using $\epsilon_{max,1} = \epsilon_{max,2} = -0.0085$ G^2/MHz, and $c_{2,max,1} = c_{2,max,2} = 7.8$ G/MHz (Table 1).

B. Simulation of EPR Spectra Using Mixed-Valence Theory. The mixed-valence [$Cu^{1.5+}$...$Cu^{1.5+}$] center was treated as a dimer built from two interacting monomeric sites Cu_{A1} and Cu_{A2}. As described in the supporting information, the system **g** and Cu hyperfine tensors are influenced in a characteristic way by the local geometries around the Cu atoms. In agreement with Westmoreland et al.,[54] the **g** tensor is constructed as a delocalization weighted sum of the hypothetical **g** tensors for

(51) Martin, C. T.; Scholes, C. P.; Chan, S. I. *J. Biol. Chem.* **1988**, *263*, 8420.

(52) Gurbiel, R. J.; Fann, Y. C.; Surerus, K. K.; Werst, M.; Musser, S. M.; Doan, P.; Chan, S. I.; Fee, J. A.; Hoffman, B. M. *J. Am. Chem. Soc.* **1993**, *115*, 10888.

(53) (a) Piepho, S. B.; Krausz, C.; Schatz, P. N. *J. Am. Chem. Soc.* **1978**, *199*, 2996. (b) Wong, K. Y.; Schatz, P. N.; Piepho, S. B. *J. Am. Chem. Soc.* **1979**, *101*, 2793. (c) Schatz, P. N. *Mixed Valence Compounds*; Brown, D. B., Ed.; D. Reidel Publishing Company: Dordrecht, Boston, Oxford **1980**; pp 115−150.

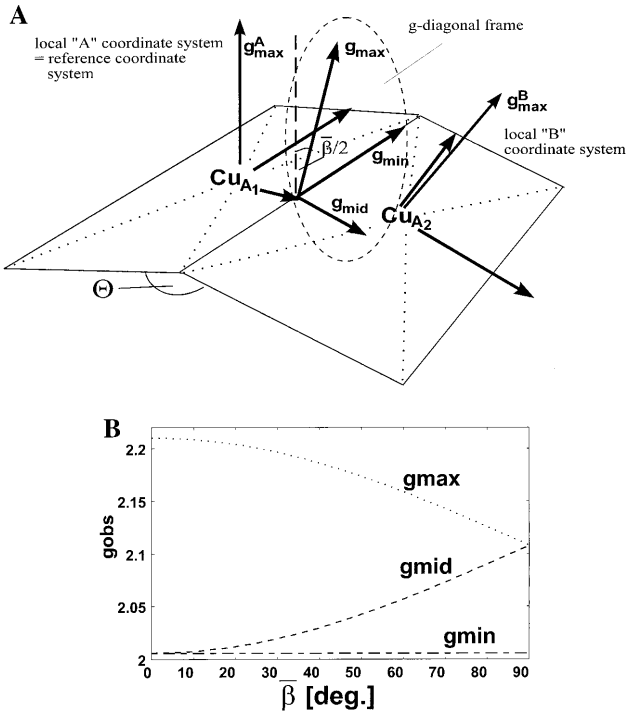

Figure 4. (A) Relationship between the g and A main axes and construction of the **g** tensor in a delocalized mixed-valence [$Cu^{1.5+}$...$Cu^{1.5+}$] site from hypothetical subsite **g** tensors of Cu_{A1} and Cu_{A2}. (B) Variation of observable g values as a function of the angle ($\Theta = 180° - \bar{\beta}$), which is defined by the tilt of the two subsite g_{mid}/g_{min} planes.

the monomeric sites (Figure 4). However, in adding the two contributions, a common frame of reference must be used. Any noncollinearity in the local tensor main axis systems leads to a reorientation of the global (observable) **g** tensor. This will introduce a noncollinearity between the system **g** and Cu hyperfine tensor systems. While the matter of introducing local g values is arbitrary, the tilt of the g and A axes is not. If two monomers with axial EPR parameters were used as a starting point, an alignment which introduced an angle $\Theta = 180° - \bar{\beta}$ between the two planes defined by the local g_I directions led to the following observable g values (eqs 5a−c):

$$g_1^{obs} = \frac{1}{2}(g_x + g_z) + \frac{1}{2}\cos(\bar{\beta})(g_x - g_z) \quad (5a)$$

$$g_2^{obs} = g_y \quad (5b)$$

$$g_3^{obs} = \frac{1}{2}(g_x + g_z) + \frac{1}{2}\cos(\bar{\beta})(g_z - g_x) \quad (5c)$$

The hyperfine tensors were tilted at angles $\pm(1/2)\bar{\beta}$ with respect to the main axes of the **g** tensor. This second set of simulations was based on delocalization weighted sums of two tensors from monomeric Cu sites. A slightly better fit to the second-harmonic X-band spectrum of $^{15}N/^{65}Cu$ N_2OR was obtained by using $\bar{\beta} = 35°$ (Figure 4). The relative intensities of the high-field lines were better represented by this approach than by using collinear **g** and **A** tensors. The parameters for the hypothetical monomers are given in Table 2.

Interpretation of Spin Hamiltonian Parameters. For monomeric Cu(II) sites with axial symmetry, and the hole in the mainly Cu-$|x^2 - y^2\rangle$ MO, Maki and McGarvey have derived expressions for the spin Hamiltonian parameters from MO theory.[55] A simplified version of these equations is given by eqs 6a−d. ζ_{3d}^{Cu} is the one-electron spin−orbit coupling constant for the Cu(II) 3d wave functions (828 cm^{-1}), $-P_{3d}^{Cu}\kappa$ is the isotropic part of the copper hyperfine interaction, α^2 is the spin density in the Cu-$|x^2 - y^2\rangle$ orbital, β_1^2 is the spin density in the Cu-$|xy\rangle$ AO in the excited state (at energy Δ_{xy} above the ground state) where one electron has been promoted from the predominantly Cu-$|xy\rangle$ MO into the predominantly Cu-$|x^2 - y^2\rangle$ MO, and $P_{3d}^{Cu} = g_e g_{Cu} \beta_e \beta_{Cu} \langle r^{-3} \rangle_{3d}^{Cu}$. Similarly, β^2 is the Cu-$|xz, yz\rangle$ spin density in the excited state (at energy $\Delta_{xz,yz}$ above the ground state), with the unpaired electron promoted from the predominatly Cu-$|xz, yz\rangle$ MOs into the predominantly Cu-$|x^2 - y^2\rangle$ MO. Note that the equations only apply in the limit of ζ_{3d}^{Cu}/Δ small enough to justify a perturbation treatment. For the case of sufficiently small rhombicity these eqs can serve as a first approximation to the spin Hamiltonian parameters of mixed-valence Cu dimers with the hole in the predominantly Cu-$|A_1; x^2 - y^2\rangle$ − $|A_2; x^2 - y^2\rangle$ MO (b_{3u} symmetry in D_{2h}; Figure 5) if the following identifications are made: Δ_{xy} is the excitation energy into the hole state where the unpaired electron residues in the predominantly Cu-$|A_1; xy\rangle$ − $|A_2; xy\rangle$ MO (b_{2u} symmetry in D_{2h}; Figure 5). Each Cu equally contributes 50% to α^2, β^2, and β_1^2, and the hyperfine coupling constants have to be divided by 2. g_I will be split into g_{mid} and g_{min}, and the excitation energies refer to the predominantly Cu-$|A_1; xz, yz\rangle$ − $|A_2; xz, yz\rangle$ hole states (b_{1u} and a_u in D_{2h}; Figure 5).

$$g_{||} = g_e + 8\zeta_{3d}^{Cu}\alpha^2\beta_1^2/\Delta_{xy} \quad (6a)$$

$$g_{\perp} = g_e + 2\zeta_{3d}^{Cu}\alpha^2\beta^2/\Delta_{xz,yz} \quad (6b)$$

$$A_{||} = P_{3d}^{Cu}\left[-\frac{4}{7}\alpha^2 - \kappa + (g_{||} - g_e) + \frac{3}{7}(g_{\perp} - g_e)\right] \quad (6c)$$

$$A_{\perp} = P_{3d}^{Cu}\left[\frac{2}{7}\alpha^2 - \kappa + \frac{11}{14}(g_{\perp} - g_e)\right] \quad (6d)$$

Various combinations having been tested for the absolute and relative signs of the measured Cu hyperfine values, the best fit was obtained with $\alpha^2 = 0.31$, $A_{iso} = -249$ MHz (83×10^{-4} cm^{-1}) for the first simulation set, and $\alpha^2 = 0.37$, $A_{iso} = -240$ MHz (80×10^{-4} cm^{-1}) for the second set; for P a value of 1187 MHz (396×10^{-4} cm^{-1}) was used.[56] Note that each Cu center contributes only 50% to the value of α^2. Both sets of values imply a strong delocalization of the unpaired electron onto the neighboring groups, most likely thiolate sulfur atoms. This effect appears to be even more pronounced in the type-1 Cu sites ($\alpha^2 = 0.41$[6]), which are known to be highly covalent.[57−59]

Table 2. Best Fit Parameters for the Simulation of the X-Band EPR Spectrum of ^{65}Cu- and [^{15}N]Histidine-Enriched N_2OR from *P. stutzeri*[a]

	g	$\mathbf{A}^{Cu}$ (MHz)	W (G)	c_2 (G/MHz)	ϵ (G^2/MHz)
g_{min}	2.003	105	13.0	1.0	−0.002
g_{mid}	2.005	116	12.0	2.0	0.001
g_{max}	2.203	235	13.5	7.9	−0.0078

[a] The [$Cu^{1.5+}$...$Cu^{1.5+}$] site is described by two identical interacting monomers Cu_{A1} and Cu_{A2}; The mixing parameter $\alpha^2 = 0.51$ refers to the probability of finding the system in the state were the unpaired electron is localized on one half of the dimer; details in supporting information. Tilt angle $\bar{\beta} = 38°$ (see eq 5 and Figure 4).

(54) Westmoreland, T. D.; Wilcox, D. E.; Baldwin, M. J.; Mims, W. B.; Solomon, E. I. *J. Am. Chem. Soc.* **1989**, *111*, 6106.

(55) (a) Maki, A. H.; McGarvey, B. R. *J. Chem. Phys.* **1958**, *29*, 31, (b) 35.

(56) Gewirth, A. A.; Cohen, S. L.; Schugar, H. J.; Solomon, E. I. *Inorg. Chem.* **1987**, *26*, 1133.

(57) Penfield, K. W.; Gewirth, A. A.; Solomon, E. I. *J. Am. Chem. Soc.* **1985**, *107*, 4519.

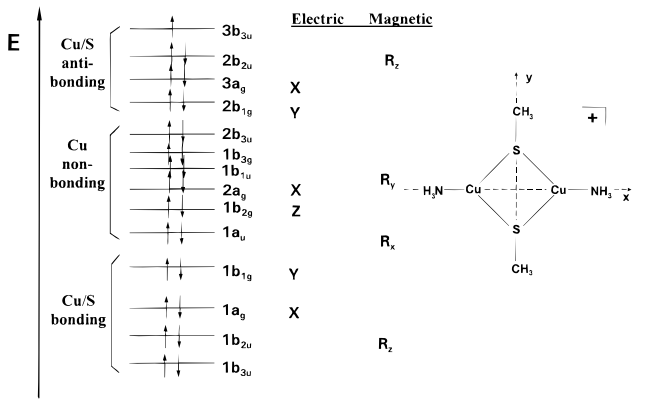

Figure 5. MO scheme of $[(H_3N)Cu^{1.5+}(SCH_3)_2Cu^{1.5+}(NH_3)]^+$ as a model for the mixed-valence $[Cu^{1.5+}...Cu^{1.5+}]$ site in N_2OR. The level ordering was obtained from an UHF-INDO/S calculation despite the interchange of the uppermost b_{2u} and b_{3u} levels. The calculated ground state is nevertheless $^2B_{3u}$ because the lowest unoccupied β-spin orbital is of b_{3u} symmetry. Energies are not at scale. The electric and magnetic dipole selection rules for the hole states obtained by exciting an electron from a doubly occupied into the singly occupied MO are indicated as well as the choice of axes. Note that all atomic orbitals referred to in the text are relative to local axes which are collinear with the global frame of reference in the figure. Distances and angles: Cu−Cu, 2.46 Å; Cu−S, 2.20 Å; Cu−N, 1.90 Å (EXAFS[72]); S- - -S, 3.68 Å; Cu−S−Cu, 68°; S−Cu- - -Cu, 112° (calculated); S- - -S−C, 109.47° (tetrahedral, assumed).

This arises despite the fact that twice the value of A_{max} found for Cu_A (≈240 MHz; Table 1) is on the upper end of the A_{max} values found in blue proteins (≈190 MHz[59]) since the positive orbital dipolar contribution in eq 6c counteracts the negative spin-dipolar and isotropic terms to a lesser extent in Cu_A due to the smaller g shift ($g_{max} = 2.18$ for Cu_A compared to 2.23 for plastocyanin).

In the case where the state which contributes most to the shift of g_{max} is close in energy to the ground state, a treatment using perturbation theory will be most likely inappropriate.[60] The g shift should be calculated with the more general formula (eq 7).

$$g_{max} = g_e + \frac{8\alpha^2\beta_1^2\zeta_{3d}^{Cu}(\Delta_{xy} + \sqrt{\Delta_{xy}^2 + 4\alpha^2\beta_1^2(\zeta_{3d}^{Cu})^2})}{\Delta_{xy} + 4\alpha^2\beta_1^2(\zeta_{3d}^{Cu})^2 + \Delta_{xy}\sqrt{\Delta_{xy}^2 + 4\alpha^2\beta_1^2(\zeta_{3d}^{Cu})^2}} \quad (7)$$

Assuming $\beta_1^2 = \alpha^2$ (the spin density in the predominantly Cu-$|A_1; xy\rangle - |A_2; xy\rangle$ hole state is identical to that in the ground state, vide infra), the equations can be solved for the excitation energy Δ_{xy}, giving $\Delta_{xy} = 3500$ cm^{-1} and $\Delta_{xy} = 4500$ cm^{-1} for the first and second sets of simulations. Thus, our analysis predicts an electric dipole forbidden transition in the near-infrared region of the electronic spectrum of Cu_A. Such a transition, however, has not been detected yet.

Molecular Orbital Calculations. Type-1 Cu in Plastocyanin. To test our approach, we carried out calculations on plastocyanin, which has been well characterized spectroscopically and theoretically by Solomon and co-workers.[57−59,61] The results of our calculations depended to some extent on the Hückel parameter K. For $K = 2.5$ and $k = 0.1$ (eq 4) we obtained a SOMO which was similar to that described by Lowery and Solomon[48] using the more elaborate SW-Xα (scattered wave formalism with local Xα electron exchange potential) method. The calculated orbital splitting pattern was close to what one would expect for a site of C_{3v} symmetry and was consistent with the assignment of optical transitions by Gewirth and Solomon.[58] The SOMO consisted of 41% Cu 3d with minor admixtures of Cu $4p_{x,y}$, 42% S_{Cys} 3p, 4.2% and 4.6% N_{1His} and N_{2His} σ-orbitals, and a negligible contribution (<1%) of the methionine sulfur orbitals. Using the approach of Stone,[62] the **g** tensor of the type-1 Cu was calculated, and with the formula of Keijzers and DeBoer,[15,63,64] the hyperfine tensors for the β-protons of cysteine and the imidazole nitrogen atoms of histidine were obtained. The results shown in Table 3 are in good agreement with the experimental data.[15,68,69] The proton hyperfine tensor is necessarily isotropic in our approach because the multicenter integrals had been neglected. The principal values obtained from the calculation were nevertheless in good agreement with the ENDOR results. The angular dependence of the β-proton couplings from cysteine calculated by the iterative extended Hückel method was in agreement with the empirical equation used by Werst et al.[64] to estimate sulfur spin densities from ENDOR data. The nitrogen hyperfine values calculated by this approach differed by a factor of 2 from the experimental values, which may have resulted from replacing the imidazole nitrogen of histidine (sp^2 nitrogen) by ammonia (sp^3 nitrogen). Notwithstanding, the calculated spin densities follow the expectation for nitrogen hyperfine values in ENDOR spectra.[64,65] The largest component of the nitrogen hyperfine tensor points along the Cu−N bond. The largest component of the **g** tensor points approximately along the $Cu-S_{Met}$ bond as described earlier.[66] Thus, the extended Hückel method can

Table 3. Calculated EPR Parameters for the Type-1 Cu Site in Plastocyanin[a]

	x		*y*		*z*	
	calc	exptl	calc	exptl	calc	exptl
g	2.058	2.042	2.082	2.059	2.247	2.226
$\mathbf{A}^{N1}$ (MHz)	12.6 (||Cu−N)	22 (||Cu−N)	2.9		3.1	
$\mathbf{A}^{N2}$ (MHz)	11.7 (||Cu−N)	22 (||Cu−N)	3.3		3.4	
$\mathbf{A}^{H1}$ (MHz)	24.5 (iso)	27 (iso)				
$\mathbf{A}^{H2}$ (MHz)	12.5 (iso)	16				

[a] The *z*-axis points approximately along the $Cu-S_{Met}$ bond; the *x*-axis is oriented approximately along the $Cu-S_{Cys}$ bond. Only the principal values from the diagonalization of the squared hyperfine tensor are given. The orientation of the ligand hyperfine tensors is explicitly stated. Note that the calculation involves the adjustment of the energy of the highest doubly filled MO (mainly Cu $3d_{z^2}$) at 5000 cm^{-1} below the SOMO;[63] experimental EPR parameters are from the literature.[58,64]

(58) Gewirth, A. A.; Solomon, E. I. *J. Am. Chem. Soc.* **1988**, *110*, 3811.
(59) Solomon, E. I. *The Chemistry of Copper and Zinc Triads*; Welch, A. J., Chapman, S. K., Eds.; Royal Society of Chemistry, Thomas Graham House, Science Park: Cambridge, 1993; pp 12−29.
(60) Sharnoff, M. *J. Chem. Phys.* **1965**, *42*, 3383.
(61) Solomon, E. I.; Lowery, M. D. *Science* **1993**, *259*, 1575.
(62) Stone, A. J. *Proc. R. Soc.* **1963**, *A271*, 424.
(63) (a) Hüttermann, J.; Kappl, R. *Metal Ions in Biological Systems*; Sigel, H., Ed.; Marcel Dekker Inc.: New York, Basel, 1987; Vol. 22, pp 1−80. (b) Hüttermann, J. *Biological Magnetic Resonance*; Berliner, L. J., Reuben, J., Eds.; Plenum Press: New York, London, 1993; Vol. 13, pp 219−252.
(64) Werst, M. M.; Davoust, C. E.; Hoffman, B. M. *J. Am. Chem. Soc.* **1991**, *113*, 1533.
(65) Hoffman, B. M. *J. Am. Chem. Soc.* **1993**, *115*, 10888.
(66) Penfield, K. W.; Gay, R. R.; Himmelwright, R. S.; Eickmann, N. C.; Norris, V. A.; Freeman, H. C.; Solomon, E. I. *J. Am. Chem. Soc.* **1981**, *103*, 4382.
(67) (a) Harding, C.; McKee, V.; Nelson, J. *J. Am. Chem. Soc.* **1991**, *113*, 9684. (b) McKee, V. *Adv. Inorg. Chem.* **1993**, *40*, 323;
(68) (a) Hathaway, B. J.; Billing, D. E. *Coord. Chem. Rev.* **1970**, *5*, 143. (b) Hathaway, B. J. *Coord. Chem. Rev.* **1983**, *52*, 87. (c) Hitchman, M. A. *Comm. Inorg. Chem.* **1994**, *15*, 197.
(69) Blackburn, N. J.; Barr, M. E.; Woodruff, W. H.; van der Oost, J.; de Vries, S. *Biochemistry* **1994**, *33*, 10401.

be used with caution to predict magnetic parameters of highly covalent Cu sites of low symmetry.

MO Calculations. Mixed-Valence Dicopper(I,II) Complex $[Cu_2L]^{3+}$. The structurally well characterized Cu(I),Cu(II) complex $[Cu_2L]^{3+}$, {L = $N[CH_2CH_2N(H)CH_2CH_2N(H)CH_2CH_2]_3N$},[49,67] was analyzed as a model for a delocalized mixed-valence site. When we used an idealized D_{3h} symmetry and inserted the bond length obtained from the crystal structure, the SOMO was mainly represented by an antisymmetric combination of the metal d_{z^2} orbitals (a_{2u} symmetry), which is in line with the Fenske−Hall calculations of Barr et al.[49] It can be shown[44] that the $^2A_{2u}$ ground state leads to $g_z = g_e$, and $g_x = g_y > g_e$, i.e., the **g** tensor symmetry is similar to what one expects for a copper monomer with trigonal bipyramidal geometry (predominantly d_{z^2} SOMO).[68] With the same parameters as used before for the calculation of the type-1 Cu in plastocyanin, the values $g_z = 2.002$ and $g_{x,y} = 2.14$ were obtained, which are again in good agreement with the experimentally obtained values of $g_z = 2.002$ and $g_{x,y} = 2.125$.[44,49] The calculated spin density distribution is 32% on each copper and 9.8% on the axial and 2.7% on the equatorial nitrogens.

MO Calculations. $[Cu^{1.5+}...Cu^{1.5+}]$ Site in Nitrous-oxide Reductase. Several structural models have been proposed for the $[Cu^{1.5+}...Cu^{1.5+}]$ site in N_2OR and COX over the years including a thiolate sulfur-bridged copper dimer and a dimer with a Cu−Cu bond.[1,15,29,32,69,70] Molecular biology was also decisive in determining the coordination of Cu_A in N_2OR,[25,29,32,71] i.e., two cysteines and two histidines as major ligands. Most recent crystallographic data[12,13] on Cu_A in COX reveal a structure where two thiolate sulfur atoms from cysteine bridge the two Cu centers. In our calculations an idealized, planar $[(NH_3)Cu^{1.5+}(SCH_3)_2Cu^{1.5+}(NH_3)]^+$ core was used. The orbitals for this site were labeled with D_{2h} symbols although the actual symmetry is somewhat lower (C_i). Furthermore, bond lengths obtained from EXAFS experiments were inserted.[21,69,72] The short Cu−Cu distance of 2.46 Å and the Cu−S distance of 2.20 Å[72] led to a S−Cu−S angle of 110° while the Cu−S−Cu angle was around 70° with a S−S distance of 3.6 Å (Figure 5). With this configuration the IEHT and UHF-INDO/S calculations showed that the two in-plane orbitals of each sulfur atom interacted strongly with the two in-plane orbitals of each Cu atom to form the covalent $[(NH_3)Cu^{1.5+}(SCH_3)_2Cu^{1.5+}(NH_3)]^+$ site. A characteristic energy scheme consisting of eight MOs emerged where four Cu−S bonding orbitals are stabilized and four Cu−S antibonding orbitals are destabilized; six orbitals, which are essentially pure metal orbitals, remain nonbonding (Figure 5). The ground state electronic configuration was not an obvious choice. However, one of the potential ground states, $^2B_{2u}$, was associated with very little spin density on the coordinated nitrogens because the symmetric and antisymmetric combinations of the nitrogen-donor orbitals transform under the a_g and b_{3u} irreducible representations of D_{2h} and therefore cannot combine with a metal b_{2u} fragment orbital. This contradicts the experimental value of 3−5% spin density on N_{His} obtained by ENDOR for both N_2OR[73] and COX.[52] In the IEHT calculations the spin density distribution contained 64% Cu character and 28% S character vs 38% (Cu) and 44% (S) predicted by UHF-INDO/S. Apparently the UHF-INDO/S values are in better agreement with the EPR parameters. The spin density in the $^2B_{2u}$ state, which was associated with the g_{max} shift, was calculated to be 30% (Cu) and 56% (S). As indicated in the MO scheme (Figure 5) both the $^2B_{2u}$ and the $^2B_{3u}$ ground state will lead to the experimentally observed order $g_{max} > g_{mid} \approx g_{min}$, with g_{max} along the normal of the Cu−SS−Cu plane. This can be understood when considering that in both states the motion of the unpaired electron is largely confined to the Cu−SS−Cu plane. This is equivalent to a small electric current which gives rise to a magnetic moment perpendicular to this plane (Figure 6). By means of ΔSCF-INDO/S calculations on a planar $[(NH_3)Cu^{1.5+}(SCH_3)_2Cu^{1.5+}(NH_3)]^+$ site we found that the $^2B_{2u}$ state lies only about 900 cm^{-1} above the $^2B_{3u}$ state compared to 3.500−4.500 cm^{-1} obtained from the analysis of the g values above (ΔSCF, the difference between two separate self-consistent field calculations). Perhaps there is a significant deviation from planarity in the actual structure of Cu_A which would account for the shift in transition energy. The MO calculations showed some degree (1−5%) of $d_{xy,x^2-y^2}/p_{x,y}$ mixing. The contributions of the metal p orbitals enter with an identical sign into the expression for the spin-dipole part of the Cu hyperfine structure. Thus, they will not have a strong influence on the metal hyperfine couplings. The extent of d/p hybridization could be probed by single-crystal X-ray spectroscopy as for plastocyanin.[74]

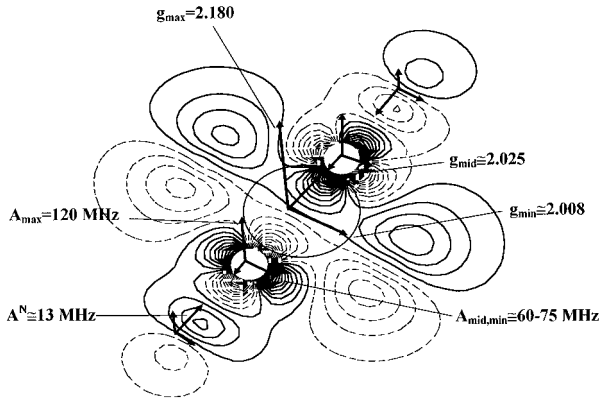

Figure 6. Contour plot (*xy* plane) of the SOMO (approximate b_{3u} symmetry) for the planar $[H_3NCu^{1.5+}(SCH_3)_2Cu^{1.5+}NH_3]^+$ site as calculated by the iterative extended Hückel theory method using $K = 2.5$ and $k = 0.1$. The relation between experimental EPR parameters and the proposed electronic structure is indicated.

In summary, the INDO/S calculations gave a satisfactory interpretation of the spin distribution when compared to experimental magnetic data. The orbital scheme found by either the INDO/S or the IEHT calculations effectively serves as a guide to the interpretation of g values (Figure 6), but the actual assignment of the ground state for Cu_A must remain uncertain at this stage.

Discussion

EPR Parameters. The results of the isotopic substitution experiments clearly show that the seven-line pattern in the CW EPR spectra of the mixed-valence $[Cu^{1.5+}...Cu^{1.5+}]$ center in N_2OR originates from an unpaired electron interacting with two Cu nuclei. Nitrogen hyperfine splittings contribute to the EPR line width but were not resolved at any microwave frequency. Thus, all resolved hyperfine structure must belong to the two copper ions. Simulations of the EPR spectra by fitting the spectra to the spin Hamiltonian and by applying mixed-valence theory were used to determine the spin Hamiltonian parameters. While g_{max} and A_{max} were obtained accurately by this procedure, the percentage error in the numbers for g_{min}/g_{mid} and A_{min}/A_{mid}

(70) Pfenninger, S.; Antholine, W. E.; Barr, M. E.; Hyde, J. S.; Kroneck, P. M. H.; Zumft, W. G. *Biophys. J.* **1995**, *69*, 2761.
(71) Dreusch, A.; Zumft, W. G. Unpublished results.
(72) Charnock, J.; Neese, F.; Garner, D.; Zumft, W. G.; Kroneck, P. M. H. Manuscript in preparation.
(73) Kappl, R.; Neese, F.; Hüttermann, J.; Zumft, W. G.; Kroneck, P. M. H. Manuscript in preparation.
(74) Shadle, S. E.; Penner-Hahn, J. E.; Schugar, H. J.; Hedman, B.; Hodgson, K. O.; Solomon, E. I. *J. Am. Chem. Soc.* **1993**, *115*, 767.

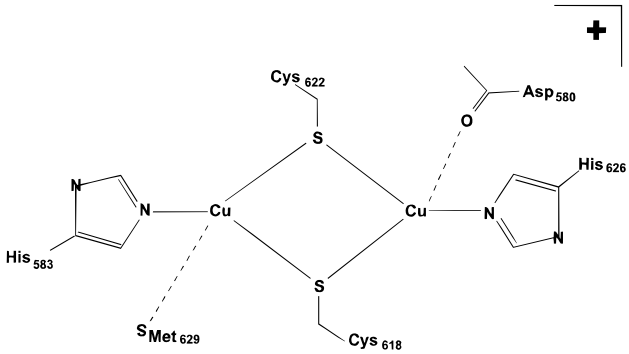

Figure 7. The Cu_A center in N_2OR. The ligand assignment is based primarily on the crystallographic data of Cu_A[12,13] in COX and amino acid sequence alignments.[25]

is likely to be higher, because only 9 out of 32 lines were resolved in the g_I region of the second-harmonic X-band EPR spectrum. The interpretation is further complicated by a possible noncollinearity of both the **g** and $\mathbf{A}^{Cu}$ tensors (Figure 4). Both analyses of metal hyperfine splittings point to a high degree of covalency in the Cu−S bonds.

Structural Model for [$Cu^{1.5+}$...$Cu^{1.5+}$]. The EPR data presented in this work including preliminary results from ENDOR and EXAFS experiments have been combined with MO calculations to build a structural model for the Cu_A center of N_2OR (Figure 7). The electronic structure in conjunction with the MO scheme of the $[(NH_3)Cu^{1.5+}(SCH_3)_2Cu^{1.5+}(NH_3)]^+$ moiety (Figure 5) leads to a reasonable interpretation for the EPR data of $[Cu^{1.5+}...Cu^{1.5+}]$. A significant result of the analysis developed in the present paper, and which has to be tested in future experiments, is the prediction of a magnetic dipole *z*-polarized and electric dipole forbidden absorption band in the region 3500−4500 cm^{-1}. The calculations of the electronic structure based on experimental results from the multifrequency EPR data and the ENDOR and EXAFS data of others cannot unequivocally distinguish between the sulfur-bridged mixed-valence dimer (Figure 7) and a nonbridged structure with a Cu−Cu metal bond.[69] Thus, knowledge of the crystal structure in combination with more refined MO calculations and spectroscopy on single crystals of proteins containing the Cu_A center is imperative for a complete understanding of the unique spectroscopic properties of the $[Cu^{1.5+}...Cu^{1.5+}]$ site. Its position in the Peisach−Blumberg plot of g_{II} vs A_{II}[17] is primarily caused by the apparent small value of A_{II}. However, a correct comparison between the delocalized mixed-valence $[Cu^{1.5+}...Cu^{1.5+}]$ site and mononuclear Cu centers in this plot requires multiplication of the A_{II} value by 2, which is directly related to the fact that the unpaired electron spends only half of its time on each half of the dimer. Then the position of Cu_A in the Peisach−Blumberg diagram comes closer to the domain of type-1 Cu, being only slightly displaced because of its low g_{II}. Considering the magnitude of g_{II} in terms of geometrical effects (Figure 4), a **g** tensor of 2.20 (for a hypothetical monomer) is more appropriate. The remaining differences may result from a more pronounced covalency of the purple Cu_A center compared to the blue type-1 Cu center. It appears that even though each Cu atom is likely to be coordinated by two thiolate sulfurs from cysteine, the reduction of the g and A^{Cu} values is approximately equivalent to a situation where each Cu atom has only one sulfur in its coordination sphere. This is understandable when one considers that the Cu:S ratio is 1:1. Each of the cysteinates bound to copper has a bond strength half of that of the $Cu-S_{Cys}$ bond in a type-1 Cu center such as in plastocyanin.

Most recently, Larsson et al.[75] carried out CNDO/S calculations of optical spectra of Cu_A in COX and proposed an unbridged structure. Their main argument was based on the lack of calculated intensity in the near-IR region at 12 000 cm^{-1} for a sulfur-bridged dimer. From the energy diagram of $[(NH_3)Cu^{1.5+}(SCH_3)_2Cu^{1.5+}(NH_3)]^+$ (Figure 5) at least two allowed electric dipole transitions of opposite polarization ($^2B_{3u} \rightarrow {}^2B_{1g}$, $^2B_{3u} \rightarrow {}^2A_g$) at lower energy are predicted. A detailed study of the excited states of Cu_A is the subject of a separate publication.[76]

Acknowledgment. We are grateful to Hartmut Michel, So Iwata, Matthias Wilmanns, and Matti Saraste for providing results in advance of publication. We thank Helmut Beinert for helpful discussions and his continuous interest in this project and Petra Majer for skillful technical assistance. The work was supported by Deutsche Forschungsgemeinschaft and Fonds der Chemischen Industrie (F.N., P.M.H.K., W.G.Z.) and the National Science Foundation (W.E.A., P.M.H.K., DMB-9105519). We thank the Stable Isotope Resource at Los Alamos National Laboratory for providing the ^{15}N-enriched histidine (supported by NIH Grant No. RR02231, under the auspices of the U.S. Department of Energy).

Supporting Information Available: Theoretical expressions used for simulation of EPR spectra (7 pages). See any current masthead page for ordering and Internet access instructions.

JA960125X

(75) Larsson, S.; Källebring, B.; Wittung, P.; Malmström, B. G. *Proc. Natl. Acad. Sci. U.S.A.* **1995**, *92*, 7167.

(76) Farrar, J. A.; Neese, F.; Grinter, R.; Lappalainen, P.; Kroneck, P. M. H.; Saraste, M.; Zumft, W. G.; Thomson, A. J. Submitted to *J. Am. Chem. Soc.*